Lithos 162–163 (2013) 128–139

Contents lists available at SciVerse ScienceDirect

Lithos

journal homepage: www.elsevier.com/locate/lithos

Generation and evolution of siliceous high magnesium basaltic magmas in the formation of the Permian Huangshandong intrusion (Xinjiang, NW China)

Jian-Feng Gao, Mei-Fu Zhou *

Department of Earth Sciences, the University of Hong Kong, Hong Kong, China

ARTICLE INFO

Article history:
Received 26 July 2012
Accepted 4 January 2013
Available online 12 January 2013

Keywords:
Siliceous high magnesium basaltic
Permian mafic–ultramafic intrusion
Differentiation
Post-collisional environment
Huangshandong
NW China

ABSTRACT

Numerous Permian orthopyroxene-rich mafic–ultramafic intrusions in the southern margin of the Central Asian Orogenic Belt (CAOB) have been emplaced in a post-orogenic environment. The Huangshandong mafic–ultramafic intrusion is the largest in the eastern Tianshan Orogenic Belt of the CAOB and consists of a layered unit intruded by a massive unit. The layered unit consists of lherzolite, troctolite, olivine gabbro, hornblende gabbro, gabbrodiorite and diorite, whereas the massive unit is made of gabbronorite and olivine gabbronorite.

Olivine from the layered unit has Fo values of 75 to 84 and contains low NiO and MnO. Rocks from this unit have initial $^{87}Sr/^{86}Sr$ ratios (0.7031–0.7043) and ε_{Nd} values (+3.4–+7.1) while plagioclase has initial $^{87}Sr/^{86}Sr$ ratios ranging from 0.70010 to 0.71569. Olivine from the massive unit has relatively low Fo values of 59 to 70 and high NiO and MnO. Rocks from this unit have relatively low and uniform initial $^{87}Sr/^{86}Sr$ ratios (0.7030) and high ε_{Nd} values (+6.0–+7.5) and contain plagioclase with relatively low initial $^{87}Sr/^{86}Sr$ ratios (0.70042 to 0.70520). Olivines from both units have low CaO and Cr_2O_3.

Both units formed from siliceous high magnesium basaltic magmas were derived from a hydrous, depleted mantle source. Magma forming the layered unit experienced earlier removal of sulfides before emplacement, with the earlier sulfide-saturation caused by the addition of crustal material. The magma that formed the massive unit has undergone fractional crystallization of olivine ± Cr-spinel. Siliceous high magnesium basaltic magmatism, produced by melting of a hydrous depleted mantle source, may be an important feature of orogenic belts.

1. Introduction

Permian mafic–ultramafic intrusions in the Central Asian Orogenic Belt (CAOB) have been the focus of several recent studies (Gao et al., 2012; Mao et al., 2008; Pirajno et al., 2008; Qin et al., 2011; Song and Li, 2009; Su et al., 2011a,b; Wu et al., 2004; Zhang et al., 2011; Zhou et al., 2004). Although they are thought to be Alaskan type (Han et al., 2010; Su et al., 2011b), mantle plume-derived (Mao et al., 2008; Pirajno et al., 2008; Qin et al., 2011; Shan et al., 2009; Su et al., 2011a; Zhang et al., 2011) or formed in response to the asthenospheric mantle upwelling, they occur in a post-collisional environment (Gao et al., 2012; Song and Li, 2009; Wu et al., 2004; Zhou et al., 2004). A common feature of many of these intrusions is that they contain orthopyroxene and are orthopyroxene-normative (Gao et al., 2012; Shan et al., 2009; Wu et al., 2004; Zhou et al., 2004), resembling that of intrusions derived from Siliceous High Magnesium Basalt (SHMB) magmas. The Permian intrusions in the CAOB are variably mineralized with Ni–Cu sulfide and their origin, possibly linked with SHMB-like magmas, is thus important not only for the understanding of the petrogenesis of SHMB-like rocks in a post-collisional environment, but also for the genesis of Ni–Cu sulfide deposits in such an environment.

SHMB was first reported from western Australia (Redman and Keays, 1985) and rocks derived from SHMB-like magmas have subsequently been described elsewhere in the world, mostly from the Archean–Proterozoic with a few in the Phanerozoic (Arndt and Jenner, 1986; Maier and Barnes, 2010; Seitz and Keays, 1997; Sensarma et al., 2002; Srivastava, 2006, 2008; Srivastava et al., 2010; Sun et al., 1989, 1991; Wang and Zhou, 2006). These studies emphasized the orthopyroxene-normative nature and siliceous magnesian compositions of parental magmas and suggested that SHMB-like magmas may be important in the formation of magmatic Cu–Ni–(PGE) deposits in layered intrusions (Gao et al., 2012; Hoatson and Keays, 1989; Keays, 1995; Maier and Barnes, 2010; Seitz and Keays, 1997; Sun et al., 1991) and of Archean Au deposits (Keays, 1987).

The ~270 Ma Huangshandong intrusion is the largest intrusion in the eastern part of the Tianshan Orogenic Belt, southern margin of the CAOB. Previous studies have focused on the petrogenesis and Ni–Cu sulfide mineralization of the intrusion (Gu et al., 2007; Han et al., 2004; Li et al., 1996; Mao et al., 2003; Pirajno et al., 2008; Xia et al., 2010; Yang, 1996; Zhang et al., 2008; Zhou et al., 2004). Although these studies

* Corresponding author. Tel.: +852 28598251; fax: +852 25176912.
E-mail addresses: gao_jianfeng@yahoo.com (J.-F. Gao), mfzhou@hkucc.hku.hk (M.-F. Zhou).

0024-4937/$ – see front matter © 2013 Elsevier B.V. All rights reserved.
http://dx.doi.org/10.1016/j.lithos.2013.01.002

documented the considerable amounts of orthopyroxene in this intrusion, they did not address its SHMB-like geochemical affinity.

In this paper, we present new olivine compositions and whole rock geochemical data in order to constrain the nature of the parental magmas of the Huangshandong intrusion. Using this new dataset, we show that the intrusion was generated from parental magmas with SHMB-like compositions. We further demonstrate that the intrusion was formed by the injection of two magma pulses that underwent different degrees of crustal contamination with different sulfide saturation histories.

2. Geological background

The Central Asian Orogenic Belt, extending for >5000 km from the Pacific Ocean to the European Craton, is bounded by the Tarim Block and North China Craton to the south and by the Siberian Craton to the north (Fig. 1a). It is a composite orogenic belt comprising Precambrian continental fragments, island arc assemblages and oceanic crust assemblages, including ophiolites and overlying sedimentary rocks (Coleman, 1989; Jahn et al., 2000; Sengör et al., 1993; Windley et al., 2002). The southernmost part of the CAOB, the Tianshan Orogenic Belt, extends for ca. 2500 km from Xinjiang, China to Kyrgyzstan and Kazakhstan (Coleman, 1989; Gao et al., 1998; Windley et al., 1990). It is separated from the Tarim Block by the North Tarim and Xingxingxia Faults (Fig.1b). The North Tianshan and South Tianshan suture zones divide the Tianshan Orogenic Belt in the Chinese portion into the North, Middle and South Tianshan terranes from north to south (Fig.1b) (Gao et al., 1998; Windley et al., 1990). The North Tianshan terrane mainly consists of Devonian–Permian calc-alkaline volcanic and sedimentary rocks, whereas the Middle and South terranes are composed of a Precambrian crystalline basement and a sedimentary succession formed in a passive continental margin.

The eastern part of the Tianshan Orogenic Belt includes the Middle and North Tianshan terranes, separated by the Shaquanzi Fault (Fig. 2). The Middle Tianshan terrane, separated from the Tarim Block along the Xingxingxia Fault, consists mainly of Precambrian basement complexes and Proterozoic and Paleozoic granites. The North Tianshan terrane is composed of Devonian and Carboniferous strata. The lower Devonian to lower Carboniferous rocks include sandstone and pelitic slate with interlayered conglomerate, siltstone, mudstone, pyrite-bearing mudstone and limestone. The middle to upper Carboniferous strata are composed of mafic to intermediate volcanic rocks with abundant cherts and limestone, that have undergone only very low- to low-grade metamorphism. Permian granitoid plutons and mafic–ultramafic intrusions intrude the Devonian and Carboniferous strata along major faults (Fig. 2) (Li et al., 2006a; Zhou et al., 2004). Many mafic–ultramafic intrusions, particularly those along the Kangger-Huangshan Fault, host large Ni–Cu sulfide deposits (Li et al., 1996; Zhang et al., 2011; Zhou et al., 2004).

3. Field relations and petrography

The Huangshandong intrusion, north of the Huangshan Fault, is a lens-shaped body with a length of 3.5 km and a maximum width of 1.2 km, covering an area of about 2.8 km^2 (Fig. 3a). It intrudes the Carboniferous Gandun Formation of slates and volcanic tuffaceous rocks. The intrusion was originally divided into the lherzolite, gabbro-diorite and gabbronorite phases (Li et al., 1996; Zhou et al., 2004), but both the lherzolite and gabbro-diorite phases have a transitional contact and form a layered sequence. Thus, in this study the Huangshandong intrusion is divided into the layered and massive units (Fig. 3). The massive unit has a clear intrusive contact with the Carboniferous Gandun Formation (Fig. 4a) and also intrudes the layered unit (Fig. 4b).

The layered unit consists of ultramafic lherzolite and troctolite layers towards the base with more mafic olivine gabbro, hornblende gabbro, gabbrodiorite and diorite in the upper layers (Fig. 4c–d). Lherzolite contains olivine (45–80%), orthopyroxene and clinopyroxene (15–50%), hornblende (4–15%), plagioclase (1–10%) and minor biotite (1–8%). Troctolite is distributed locally along the contact between lherzolite and gabbro and consists of olivine (60–75%), plagioclase (20–

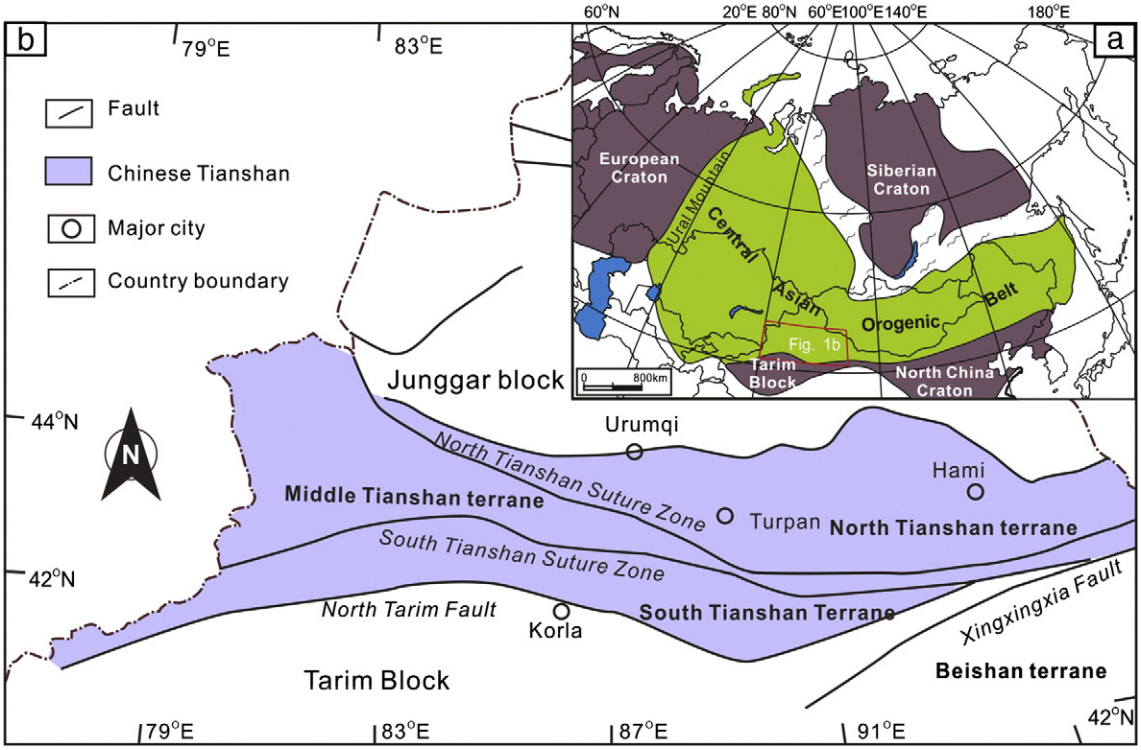

Fig. 1. a) Simplified geological map showing the location of the CAOB; b) geological map of the eastern Tianshan Orogenic Belt. Modified after Ma et al. (1997).

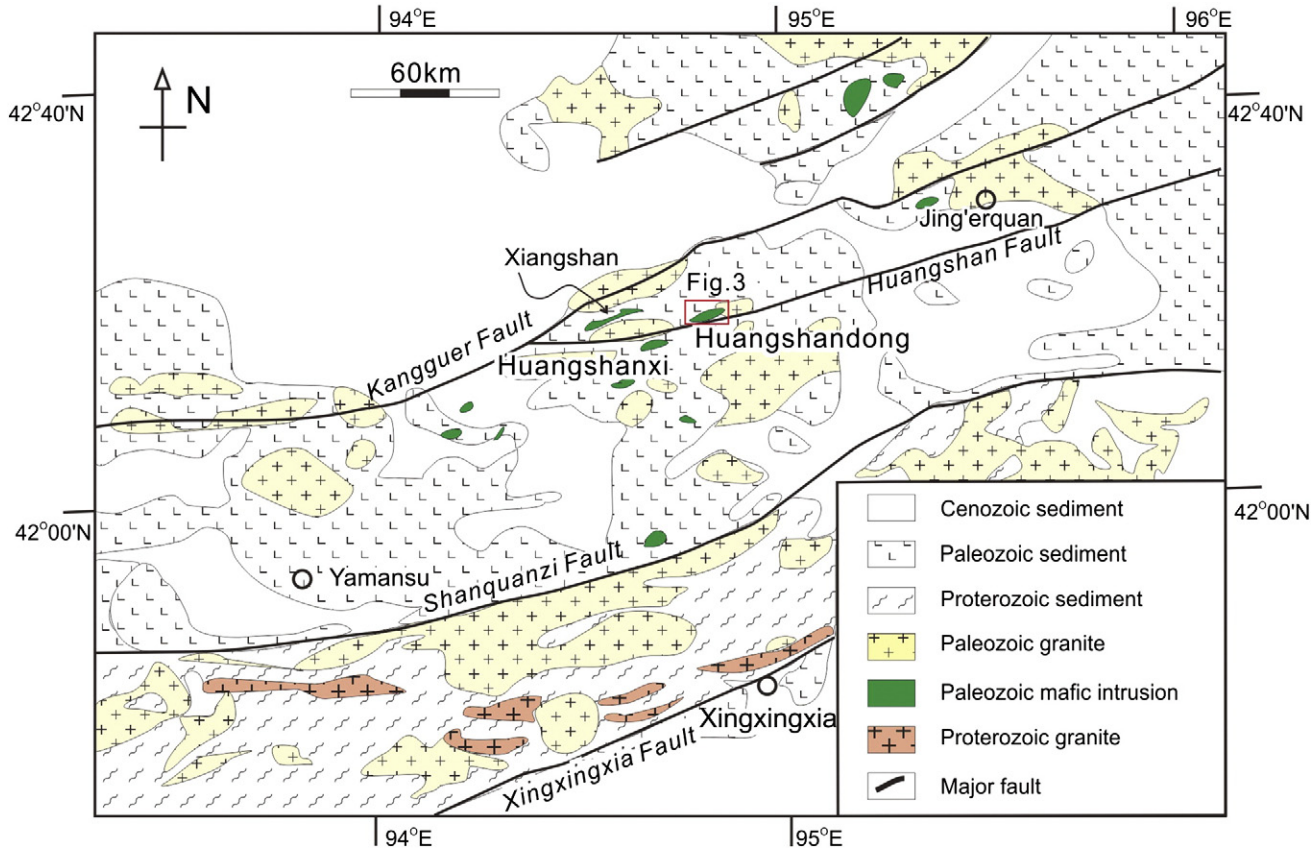

Fig. 2. Simplified geological map of the Huangshan area.
After Wang et al. (2006b).

30%) and minor orthopyroxene and Cr-spinel. Olivine gabbro comprises plagioclase (50–70%), clinopyroxene (20–30%), olivine (5–10%) and hornblende (5–10%). Hornblende gabbro is composed of plagioclase (25–60%), clinopyroxene (30–60%), olivine (0–5%) and hornblende (5–10%). Gabbrodiorite and diorite contain plagioclase (40–70%), hornblende (20–25%), biotite (5–15%) and quartz (5–10%). Biotite is mostly altered to chlorite and olivine grains in the layered unit are generally anhedral.

The massive unit comprises olivine gabbronorite and gabbronorite. Olivine gabbronorite makes up of plagioclase (40–50%), orthopyroxene (20–30%), clinopyroxene (15–20%), olivine (5–10%) and minor hornblende (<5%). Gabbronorite contains plagioclase (40–60%), orthopyroxene (20–30%) and clinopyroxene (10–30%) with minor hornblende and quartz (<5%). Olivine and pyroxene in the massive unit are euhedral to subhedral, whereas hornblende, biotite and quartz are subhedral to anhedral.

4. Analytical methods

All samples were collected from two drill holes, ZK24 + 1 from the western part and ZK20-2 from the eastern part of the intrusion, and an underground adit that was excavated for mining the sulfide ores in the middle part of the Huangshandong intrusion.

4.1. Mineral compositions

Chemical compositions of olivine were determined with a JEOL JXA-8100 electron microprobe at the State Key Laboratory for Mineral Deposits Research, Nanjing University. The analyses were performed with a voltage of 15 keV and a sample beam of 20 nA focused to a spot of ~2 μm in diameter. Peak and background counting times were set at 30s and 10s, respectively. Natural mineral standards were used for calibration and a PAP correction procedure was applied to the data (Pouchou and Pichoir, 1991). The detection limits are about 0.02% for major elements (>1 wt.%) and about 50 ppm for trace elements (<1 wt.%). The precision of the analyses is better than 5% for major elemental oxides and 15% for trace elements from the replicated analyses of standards.

4.2. Whole rock major and trace elements

Major element oxides and S were determined with a Thermo X-ray fluorescence (XRF) spectrometer on fused glass discs at the University of Hong Kong. The analytical precisions are better than 1% (RSD) for elements more than 1 wt.% and 5% (RSD) for those lower than 1 wt.% and S. Analytical results of standard materials are presented in Appendix A.

Trace elements were measured with a PE DRC-e inductively coupled plasma-mass spectrometry (ICP-MS) at the Institute of Geochemistry, Guiyang, Chinese Academy of Sciences (CAS), following the procedure described in Qi et al. (2000). Reference standards, GSR-10 (gabbro), BHVO-2 (basalt) and GBPG-1 (gneiss) (Appendix B), were used to monitor the trace element analyses, and RTS-1 and RTS-2 (sulfide ore tailings) were used to monitor Cu and Ni. The precision for these analyses is better than 5% (RSD).

4.3. Whole rock Sr–Nd isotopes

About 100 mg of powdered samples was dissolved in Teflon beakers with a $HF + HNO_3$ mixture acid. Sr and Nd were then separated and purified by conventional cation-exchange technique. The isotopic compositions of purified Sr and Nd solutions were measured using a Thermo Finnigan Triton TI thermal ionization mass spectrometer (TIMS) at the State Key Laboratory for Mineral Deposits Research, Nanjing University. Measured $^{87}Sr/^{86}Sr$ and $^{143}Nd/^{144}Nd$ ratios are normalized to $^{86}Sr/^{88}Sr$

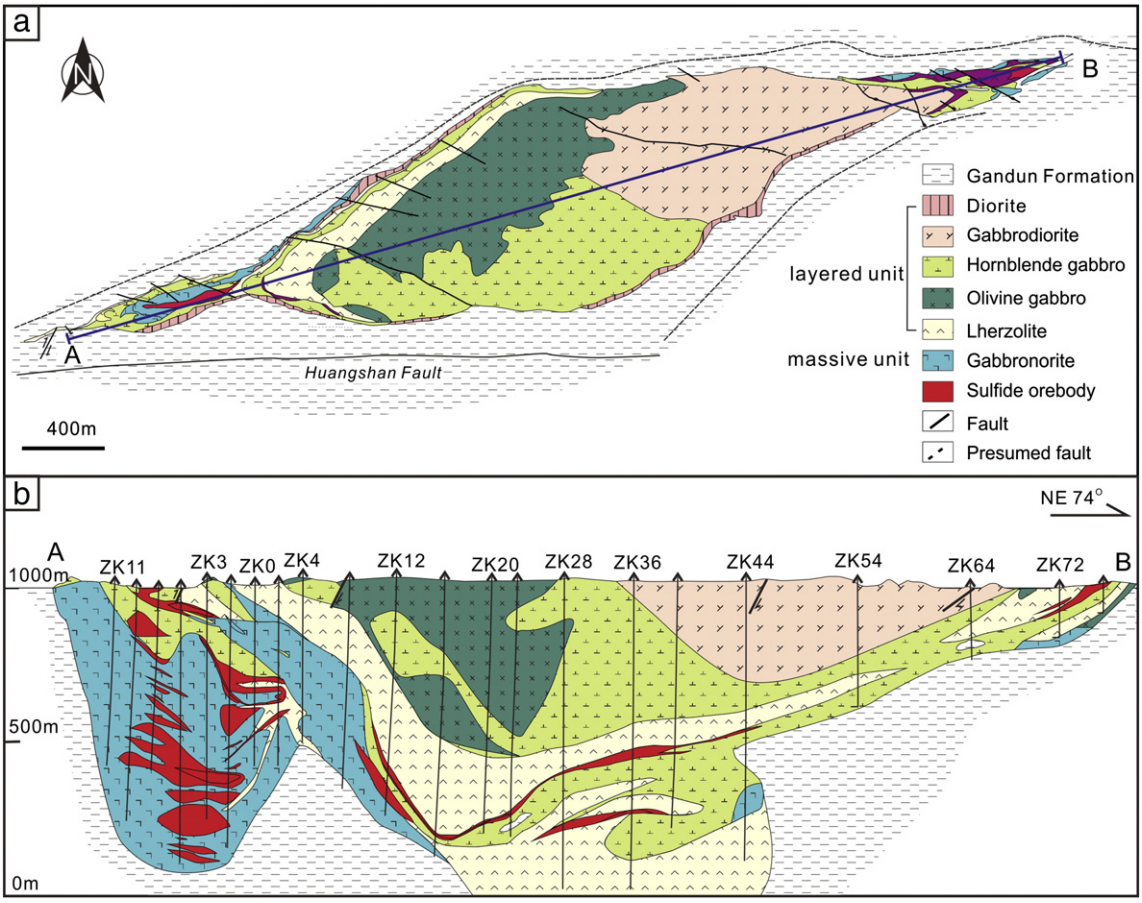

Fig. 3. a) Simplified geological map of the Huangshandong intrusion, showing the distribution of lithological units and sulfide ore bodies; b) cross section of the Huangshandong intrusion.

of 0.1194 and $^{146}Nd/^{144}Nd$ of 0.7219, respectively. Analyses of La Jolla yield an average $^{143}Nd/^{144}Nd$ ratio of 0.511842 ± 4 (2σ, n = 5), and NBS-987 gave an average $^{87}Sr/^{86}Sr$ ratio of 0.710260 ± 10 (2σ, n = 30). Total procedural blanks were 50 pg for Nd and 200 pg for Sr, respectively.

4.4. In-situ Sr isotope analyses

In-situ Sr isotopic analyses were obtained using a Resonetic M50 193 nm Excimer laser system coupled to the Nu Plasma-HR Multi Collector-Inductively Coupled plasma Mass Spectrometry (MC-ICP-MS) at the University of Hong Kong. The analytical protocol for in-situ Sr isotope analyses follows the method described in Ramos et al. (2004). Plagioclase was ablated in a mixture of helium (400 ml/min) and nitrogen (2 ml/min) atmosphere using the following parameters: 45 s ablation time, 190–140 μm spot size, 6 Hz repetition rate and 100 mJ energy. Because of the lack of internal standard, Sr contents in plagioclase cannot be analyzed precisely. The analytical accuracy for $^{87}Sr/^{86}Sr$ ratio was estimated with repeated analysis of an apatite in-house standard from Afghanistan. The average $^{87}Sr/^{86}Sr$ ratio of 29 measurements was 0.71127 ± 0.00007 (2SD), which agrees well with that obtained by in-situ LA-MC-ICP-MS (0.71137 ± 7) and that obtained by purified solution MC-ICP-MS (0.71138 ± 4) (Yang et al., 2009).

5. Analytical results

5.1. Olivine

Olivine from the layered and massive units occurs either as inclusions in pyroxene and plagioclase (Fig. 5a–d) or as discrete grains with granular or subpoikilitic pyroxene and plagioclase, and interstitial sulfides (Fig. 5b, e, f). Olivine inclusions are dominant in olivine gabbros, whereas lherzolite contains both inclusion and granular olivine grains. In most sulfide-bearing rocks, olivine is commonly altered to serpentine (Fig. 5d,e).

All olivine grains have low CaO (mostly <0.10 wt.%) and Cr_2O_3 (mostly <0.10 wt.%), but highly variable Ni and Mn contents and Fo values. Olivine grains from barren rocks from both units (HSG942 and HSG814) have low Fo values (68–76) and NiO (0.03–0.20 wt.%) (Fig. 6), and high MnO (0.33–0.49 wt.%) (Appendix C). Olivine grains from sulfide-bearing rocks in the layered unit (HSG834 and HSG968) have high Fo values (75–84) but low NiO (0.07–0.16 wt.%) and MnO (0.07–0.30 wt.%) (Appendix C, Fig. 6), whereas those from sulfide-bearing rocks in the massive unit (HSG0810 and HSG811) have low Fo values (59–70) and high NiO (0.06–0.23 wt.%) and MnO (0.22–0.70 wt.%) (Appendix C, Fig. 6). Olivine from both units forms two compositional trends in the plots of NiO vs Fo values (Fig. 6).

5.2. Whole rock major and trace elements

Whole rock major and trace elements of samples from the Huangshandong intrusion are presented in Appendix D and E, respectively. Data of major and trace elements of each unit have been summarized in Tables 1 and 2, respectively.

Rocks from both the layered and massive units have variable major element oxides, reflecting varying modal mineralogy. Major element compositions are normalized to sulfide-free composition (Table 1; Appendix D). With CIPW calculation, notably most rocks contain significant quartz (0.27–40.7%) (Table 1; Appendix D).

Rocks from the layered unit have chondrite-normalized rare earth elements (REE) patterns slightly enriched in light rare earth elements (LREE) and display variably positive Eu anomalies (Table 2;

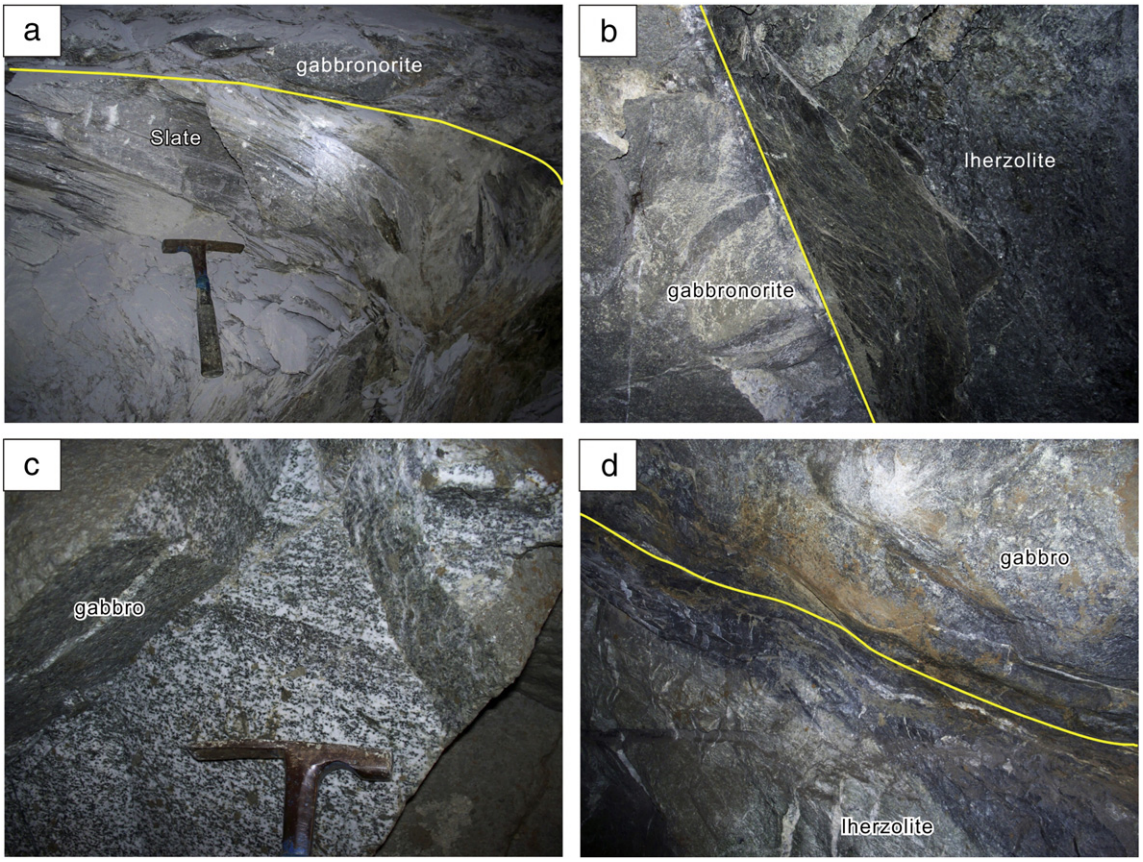

Fig. 4. a) Contact of gabbronorite and country rock (slate); b) contact of lherzolite and gabbronorite; c) magmatic layering of gabbro; d) contact of gabbro and lherzolite.

Appendix E; Fig. 7a). Some olivine gabbros from this unit are enriched in the middle rare earth elements (MREE) relative to the LREE and high rare earth elements (HREE) and therefore exhibit convex REE patterns (Table 2; Appendix E; Fig. 7a). Rocks from the layered unit have variable abundances of trace elements, they show relatively flat primitive mantle-normalized patterns, with the exception of enrichments in Cs, U and Pb and depletion in Nb (Fig. 8a). Some gabbros are enriched in Ba and Sr, whereas the other rocks and ores have no obvious Ba anomalies.

Rocks from the massive unit have near flat chondrite-normalized REE patterns and display slightly negative or positive Eu anomalies (Table 2; Appendix E; Fig. 7b). Rocks from the massive unit show similar flat primitive mantle-normalized patterns to those of the layered unit (Fig. 8b). But the layered unit has more pronounced depletion in Nb and enrichment in U than the massive unit.

5.3. Whole rock Sr–Nd isotopes

Rb–Sr and Sm–Nd isotopic data are given in Table 3. Rocks from the massive unit have low and uniform $^{87}Rb/^{86}Sr$ ratios (0.010–0.019) and initial $^{87}Sr/^{86}Sr$ ratios (~0.7030) and high ε_{Nd} values (+6.0 to +7.5), whereas rocks from the layered unit have relatively high $^{147}Sm/^{144}Nd$ ratios (0.1650–0.1981) initial $^{87}Sr/^{86}Sr$ isotope ratios (0.7031 to 0.7043) and low and highly variable $^{147}Sm/^{144}Nd$ ratios (0.1163–0.2316) and ε_{Nd} values (+3.4 to +7.1) (Table 3; Fig. 9).

5.4. In-situ Sr isotopes

In-situ $^{87}Sr/^{86}Sr$ isotopic data for plagioclase are presented in Appendix F. Plagioclase from the layered unit has highly variable Sr (^{88}Sr = 0.13 V to 0.84 V) and relatively high $^{87}Rb/^{86}Sr$ ratios (0.0005 to 0.32) and $^{87}Sr/^{86}Sr$ ratios (0.70010 to 0.71569) with initial $^{87}Sr/^{86}Sr$ ratios ranging from 0.7001 to 0.7145, whereas plagioclase from the massive unit has relatively narrow range of Sr (^{88}Sr = 0.26 V to 0.69 V) and relatively low $^{87}Rb/^{86}Sr$ ratios (0.0007 to 0.013) and $^{87}Sr/^{86}Sr$ ratios (0.70042 to 0.70520) with initial $^{87}Sr/^{86}Sr$ ratios ranging from 0.7004 to 0.7052 (Fig. 10).

6. Discussion

6.1. Low-Ca SHMB affinity of the Huangshandong intrusion

In Huangshandong, chilled margins are not observed, making it difficult to estimate the compositions of the parental magmas. However, rocks from both units are quartz-normative as all the rocks contain variable amounts of orthopyroxene. The presence of orthopyroxene indicates that the parental magmas for the Huangshandong intrusion were Si–Mg-rich (cf., Sun et al., 1989, 1991; Wang et al., 2006a).

Olivine compositions can be used to calculate MgO/FeO ratios of parental magmas, using the Mg–Fe partition coefficient of $Kd = (FeO/MgO)_{Ol}/(FeO/MgO)_L = 0.3 \pm 0.03$ (Roeder and Emslie, 1970). Using the highest Fo value (84) of olivine from the Huangshandong intrusion, the parental magma has Mg# (MgO/(MgO + FeO)) >0.61. Calculations using the MELTS program (Ghiorso and Sack, 1995) using a pressure of 0.5–2 kb and fO_2 = FMQ, yield more than 10 wt.% MgO for the equilibrated melts, consistent with high-Mg compositions.

Experiments have demonstrated that CaO contents of olivine depend on both Fo values of the olivine and melt compositions (e.g. CaO, FeO, Al_2O_3, $Na_2O + K_2O$ and SiO_2) (Libourel, 1999). Many komatiitic or high-Mg basalts with less than 12% CaO contain low Ca olivine (CaO<0.2 wt.%), whereas alkaline basalts, ferro-basalts and MORB have olivine with CaO ranging from 0.2 wt.% to 1.0 wt.% (Libourel,

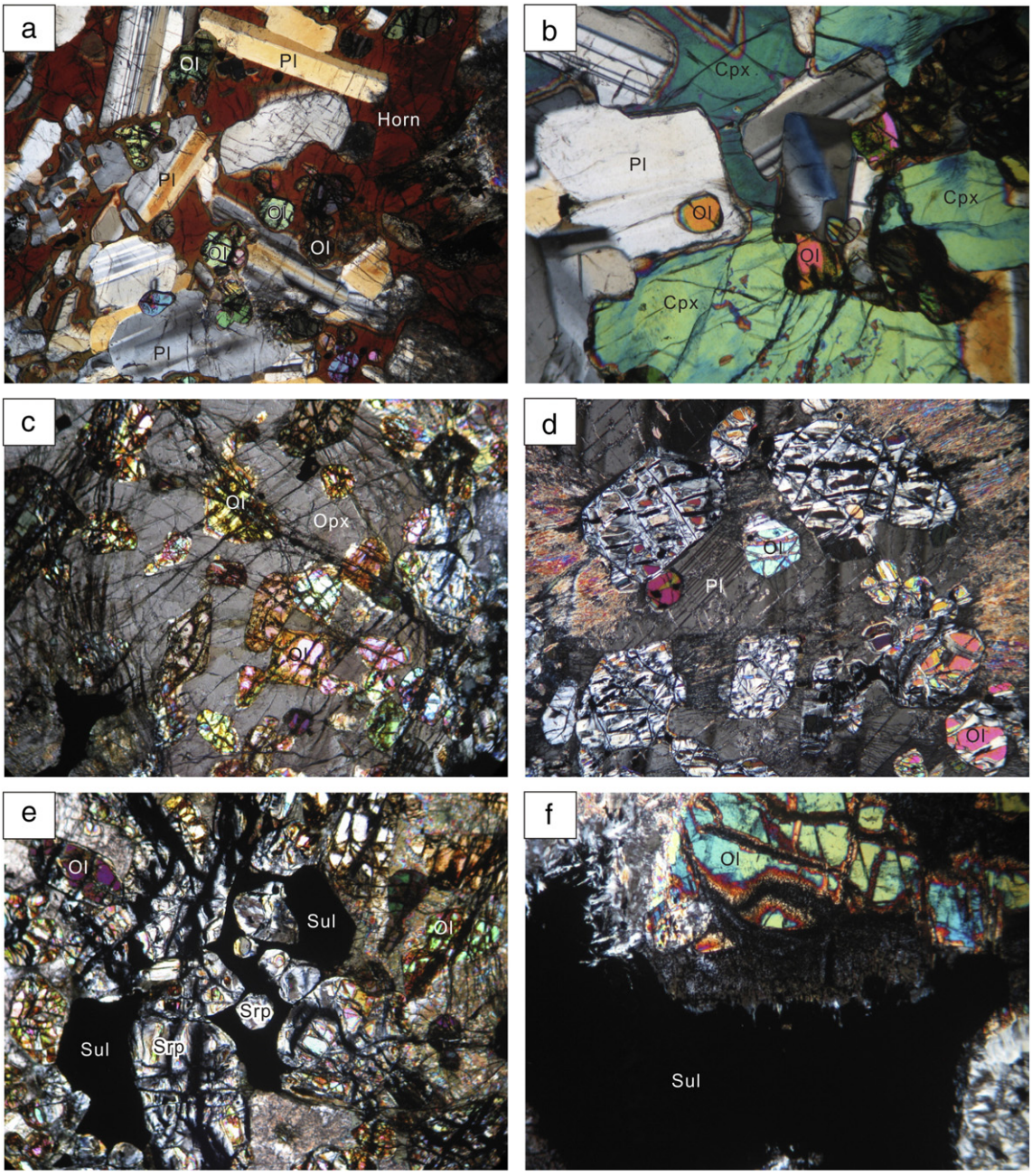

Fig. 5. Microphotographs of (a) olivine gabbro (HSG0810) (b) troctolite (HSG0811); (c) gabbro (HSG0814); (d) lherzolite (HSG0834); (e) olivine gabbro (HSG0942); (f) lherzolite (HSG0968).

1999). Most olivine grains at Huangshandong have very low CaO contents (<0.11 wt.%). Ca-poor olivine is believed either to have an origin as mantle xenocrysts or to have formed from Si-rich and Ca-poor mafic magmas (e.g., SHMB) (Boudier, 1991; Hirano et al., 2004; Kamenetsky et al., 2006; Ramsay et al., 1984). In Huangshandong, euhedral to subhedral olivine grains have Fo values less than 84 and so they cannot be mantle xenocrysts. The Huangshandong magmas had initial CaO contents of 7.7 wt.% on the basis of the formula: $CaO_{olivine} = 0.0877 * (e^{0.106 * CaO\ melt} - 1)$ (Libourel, 1999). Therefore, the Ca-poor olivine from Huangshandong was likely derived from low-Ca SHMB-like magmas.

Processes resulting in the formation of such magmas include crustal contamination and magma differentiation. Our study suggests that the magmas were derived from a hydrous, depleted lithospheric mantle source.

6.2. Crustal contamination

Assimilation with fractional crystallization (AFC) is a common magmatic process. All rocks from Huangshandong are more enriched in large-ion lithophile elements (LILE) (e.g., Cs, Rb, Ba, Sr) relative to high field strength elements (e.g., Th–Nb–Ta). The coupled enrichment in LILE and negative Th–Nb–Ta anomalies (Fig. 8) may be produced by crustal contamination during ascent and/or emplacement or subduction-related melting.

The layered unit has higher initial $^{87}Sr/^{86}Sr$ ratios and lower ε_{Nd} values than the massive unit, suggesting that the layered unit may have undergone more crustal contamination. Plagioclase are rich in Sr and can equilibrate Sr isotope with hosting magmas during magma evolution. Thus, in-situ plagioclase Sr isotope can record the petrogenetic processes (Deniel, 2009; Knesel et al., 1999; Wolff et al., 1999).

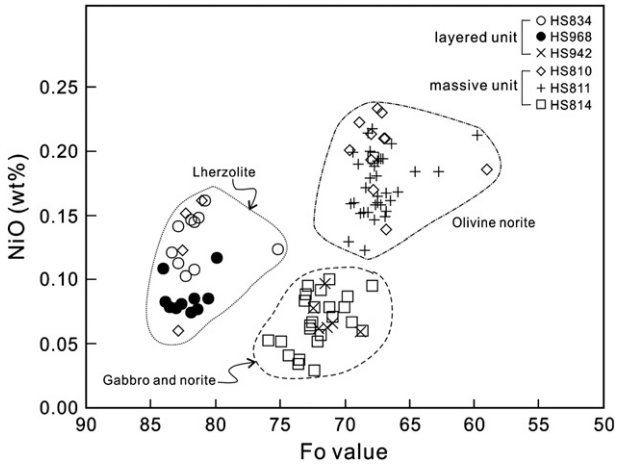

Fig. 6. Fo value vs NiO contents (wt.%) for olivine from the Huangshandong intrusion.

Plagioclase from the layered unit has highly variable $^{87}Rb/^{86}Sr$ and $^{87}Sr/^{86}Sr$ ratios, but plagioclase from the massive units has relatively uniform and low $^{87}Rb/^{86}Sr$ and $^{87}Sr/^{86}Sr$ ratios (Fig. 10), further supporting higher degrees of crustal contamination in the layered unit.

Table 1
Summary of contents of major oxides of samples from the Huangshandong intrusion.

	Massive unit				Layered unit			
	Min.	Max.	Average	SD	Min.	Max.	Average	SD
SiO_2	24.29	55.81	40.09	10.13	34.60	56.28	47.98	5.75
TiO_2	0.18	1.49	0.68	0.45	0.10	3.01	0.64	0.76
Al_2O_3	5.53	17.78	12.66	3.94	0.31	21.38	9.44	6.05
Fe_2O_3	6.46	30.30	16.77	7.89	6.00	26.20	12.38	4.60
MnO	0.06	0.14	0.10	0.03	0.07	0.23	0.14	0.03
MgO	4.41	18.65	9.35	4.30	4.61	29.58	15.06	7.38
CaO	5.04	12.59	9.03	2.32	0.70	13.66	8.58	3.42
Na_2O	0.29	3.69	1.99	1.27	0.03	4.40	1.72	1.30
K_2O	0.00	0.24	0.08	0.06	0.00	0.87	0.16	0.19
P_2O_5	0.01	1.52	0.36	0.45	0.01	1.66	0.24	0.32
S	0.31	17.15	8.39	6.04	0.05	13.89	3.49	4.29
Fe_2O_3*	3.05	9.04	6.28	1.97	0.85	13.23	8.02	3.20
Total*	60.61	99.30	80.63	13.95	68.10	99.88	91.98	9.86
Sulfide free								
SiO_2	40.08	56.27	49.11	4.93	45.10	64.30	52.25	4.05
TiO_2	0.25	1.65	0.81	0.46	0.10	3.05	0.68	0.79
Al_2O_3	7.26	19.13	15.50	3.17	0.31	23.28	10.52	6.81
Fe_2O_3	4.35	14.63	8.05	3.24	1.25	13.76	8.61	3.30
MnO	0.10	0.16	0.13	0.02	0.07	0.24	0.15	0.04
MgO	6.92	25.15	12.12	6.55	5.19	30.04	16.23	7.37
CaO	8.11	19.73	11.37	3.36	0.97	13.93	9.26	3.51
Na_2O	0.41	3.71	2.31	1.24	0.05	4.67	1.86	1.38
K_2O	0.01	0.34	0.09	0.08	0.00	0.88	0.17	0.20
P_2O_5	0.01	2.51	0.51	0.69	0.01	1.79	0.27	0.35
Normative								
Quartz	0.27	12.06	5.42	3.74	0.00	40.66	10.19	10.12
Plagioclase	17.58	64.72	46.58	15.98	1.51	77.64	31.93	23.68
Orthoclase	0.00	1.89	0.54	0.46	0.00	5.99	1.05	1.26
Corundum	0.00	2.34	0.16	0.60	0.00	6.41	0.71	1.69
Diopside	0.00	26.45	12.24	8.64	0.00	43.82	18.01	14.56
Hypersthene	0.00	42.47	18.92	12.55	6.90	54.22	30.60	15.43
Olivine	0.00	0.00	0.00	0.00	0.00	0.34	0.01	0.05
Rutile	0.00	0.00	0.00	0.00	0.00	0.00	0.00	0.00
Ilmenite	0.00	1.71	0.69	0.57	0.00	3.62	0.67	0.85
Magnetite	0.00	4.50	1.71	1.38	0.00	3.80	1.25	0.79
Hematite	0.00	2.33	0.36	0.77	0.00	1.71	0.13	0.42
Apatite	0.02	3.91	0.84	1.11	0.02	3.45	0.51	0.66
Sphene	0.00	1.33	0.14	0.36	0.00	0.22	0.01	0.04
Pyrite	0.39	27.08	12.07	9.35	0.07	20.57	4.77	6.16

Table 2
Summary of trace elements of samples from the Huangshandong intrusion.

	Massive unit				Layered unit			
	Min.	Max.	Average	SD	Min.	Max.	Average	SD
Li	0.31	12.84	3.62	2.73	0.13	19.33	6.13	5.12
Sc	0.23	30.30	15.97	9.63	0.48	51.72	14.72	11.82
V	14	212	103	54	19	423	100	85
Cr	56	1598	502	579	7	2550	979	873
Co	47	941	363	284	27	1186	243	254
Ni	211	25,420	8733	7563	12	35,582	5091	7565
Cu	130	10,700	2856	2856	33	97,357	4728	13,921
Zn	19	124	75	27	23	163	83	26
Ga	0.81	12.70	7.84	4.00	0.41	19.81	8.19	4.58
As	0.44	2.98	1.59	0.87	0.59	27.90	2.39	4.67
Rb	0.17	3.99	1.37	0.96	0.03	25.33	3.12	3.72
Sr	15	415	221	152	2	722	250	216
Y	1.04	12.27	5.71	2.98	0.48	29.01	6.49	6.03
Zr	5.5	47.7	22.1	12.6	2.4	107.0	27.6	18.4
Nb	0.16	1.39	0.60	0.42	0.08	6.60	1.09	1.25
Mo	0.21	4.26	1.35	1.19	0.17	5.01	0.99	1.07
Cs	0.04	0.65	0.33	0.21	0.00	3.59	0.57	0.58
Ba	3.4	53.9	19.4	13.0	0.9	120.8	36.0	31.2
La	0.32	3.78	1.21	0.87	0.17	10.30	2.20	1.66
Ce	0.83	7.90	3.11	1.98	0.36	24.10	5.28	4.11
Pr	0.13	1.06	0.49	0.28	0.06	3.28	0.75	0.60
Nd	0.59	4.90	2.40	1.34	0.27	15.10	3.45	2.97
Sm	0.14	1.50	0.79	0.40	0.05	4.04	0.99	0.91
Eu	0.05	0.71	0.41	0.22	0.02	1.64	0.46	0.34
Gd	0.17	1.72	0.93	0.46	0.07	4.92	1.11	1.05
Tb	0.03	0.31	0.16	0.08	0.01	0.85	0.19	0.18
Dy	0.18	1.94	0.96	0.51	0.07	4.98	1.13	1.07
Ho	0.04	0.42	0.21	0.11	0.01	1.15	0.26	0.25
Er	0.12	1.09	0.56	0.28	0.04	3.02	0.68	0.64
Tm	0.01	0.15	0.08	0.04	0.00	0.40	0.10	0.09
Yb	0.10	0.95	0.50	0.25	0.03	2.41	0.61	0.53
Lu	0.01	0.13	0.06	0.03	0.00	0.34	0.09	0.08
Hf	0.12	1.14	0.58	0.31	0.03	2.89	0.75	0.54
Ta	0.01	0.13	0.05	0.04	0.01	0.49	0.10	0.09
Pb	2.44	30.77	8.39	7.87	1.70	34.79	8.88	7.28
Bi	0.08	4.19	1.27	1.00	0.03	9.96	0.89	1.45
Th	0.01	0.69	0.13	0.16	0.01	2.94	0.37	0.42
U	0.01	0.26	0.06	0.06	0.01	1.13	0.17	0.17

6.3. Magma differentiation and sulfide saturation

The massive unit has relatively uniform values of major element oxides and show considerable fractional crystallization during the emplacement. On the other hand, the layered unit has larger variations of major elemental oxides as also reflected by the variable modal mineralogy. This variation is related to the magma differentiation involving olivine, orthopyroxene, clinopyroxene, plagioclase and Fe-oxides.

An AFC process would result in more radiogenic Sr and less radiogenic Nd isotopes in the evolved magmas. In Huangshandong, rocks from the massive unit have the most depleted isotope compositions, whereas ultramafic rocks (lherzolite) from the layered unit have more enriched compositions, suggesting these two types of rocks may have formed from different magmas rather than through a simple AFC process from a common magma (Fig. 9).

Olivine compositions further support the interpretation that two units in Huangshandong formed from different magmas. Ni contents of olivine decrease during the magma differentiation with fractional crystallization of olivine and/or sulfides, lowering both Ni contents and Fo values because Ni is comparable in olivine and sulfide (Li and Naldrett, 1999). Two compositional trends of olivine from Huangshandong suggest variable reaction between olivine and sulfide melts (cf., Li and Naldrett, 1999).

Reaction of olivine with sulfide melts would result in an inverse Ni–Fo relationship of olivine and a continuous compositional trend of Ni or Fo values with nearly constant ratios of NiO/FeO (Campbell and Roeder, 1968; Li and Naldrett, 1999; Li et al., 2003). Olivine from the Huanshandong intrusion does not have constant NiO/FeO ratios, thus,

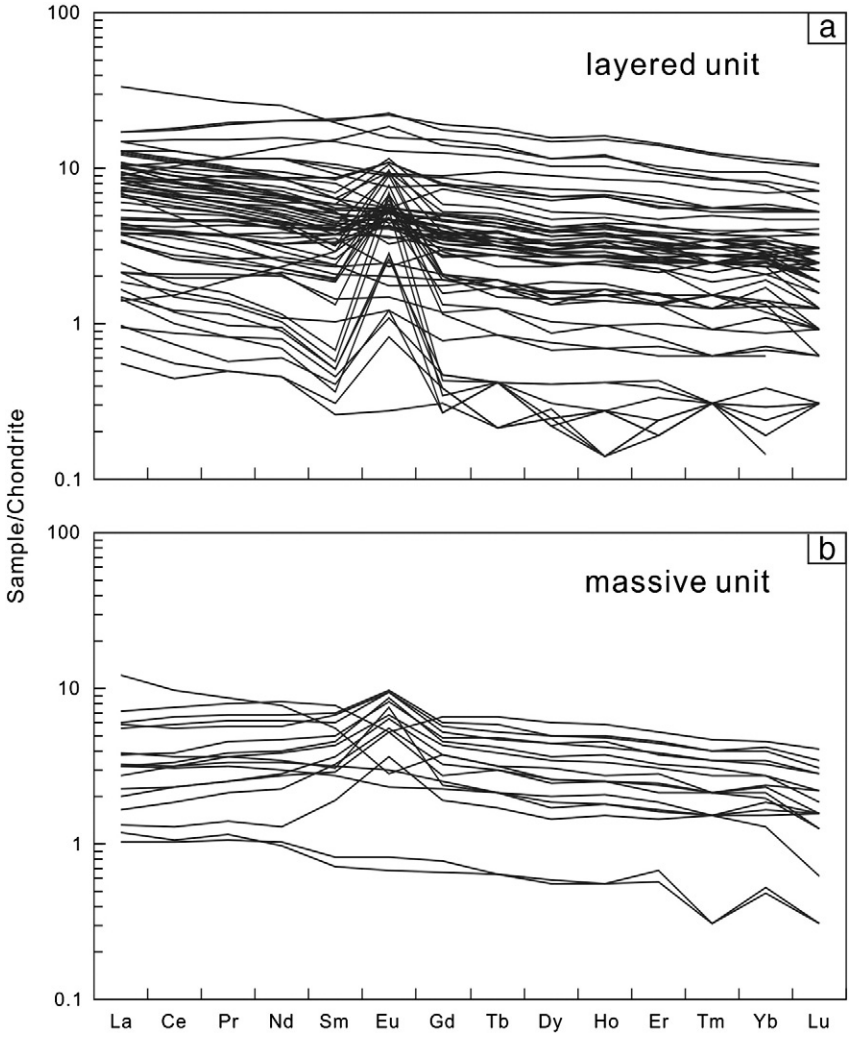

Fig. 7. Chondrite-normalized REE patterns of silicate rocks and sulfide ores (a — layered unit; b — massive unit). Normalization values are from Sun and McDonough (1989).

two parent magmas can be identified from olivine compositions. Olivine from the layered unit has high Fo values but low NiO contents and crystallized from a Mg-rich and Ni-poor magma, whereas olivine from the massive unit has relatively low Fo values but high Ni contents and formed from a relatively Mg-poor but Ni-rich magma. Both Ni and Mg are compatible in olivine, whereas Ni is compatible and Mg is incompatible in sulfides. Therefore, magmas of the layered unit might have undergone early removal of sulfide ± minor olivine. Magmas for the massive unit can be considered to be slightly evolved with fractionation of olivine without significant removal of sulfides (Fig. 11).

6.4. Melting of an hydrous, depleted mantle source

Despite the crustal contamination, rocks from both units of the Huangshandong intrusion have relatively flat chondrite-normalized REE patterns and do not show significant enrichment in Th and U. They also have relatively low and homogeneous $^{87}Sr/^{86}Sr$ ratios (0.7030 ~ 0.7043) and positive $\varepsilon_{Nd}(t)$ values (+3.4 to +7.1). Plagioclase from both the layered and massive units generally has initial $^{87}Sr/^{86}Sr$ ratios lower than 0.7040 (Fig. 10). All these geochemical features indicate that, although they underwent minor, if any, crustal contamination, a depleted mantle source can be inferred for magmas from which the Huangshandong intrusion was derived.

As the crustal contamination in the Huangshandong intrusion is insignificant, hydrous melting of mantle peridotites is a preferred mechanism for generation of the SHMB-like magmas. In Huangshandong, a hydrous magma is inferred from the existence of amphibole in the rocks. Amphibole commonly occurs in lherzolite, gabbro, norite and diorite at Huangshandong, similar to those of the Alaskan-type intrusions (Himmelberg and Loney, 1995), indicating the hydrous nature of the parental magmas. In addition, high Ba/Zr ratios of the layered unit also suggest the presence of subduction-related fluids in the parental magma.

Partial melting of mantle peridotites under water-bearing conditions would produce magmas with more siliceous and less Ca, Mg and Fe than those from similar degrees of anhydrous partial melting (Jaques and Green, 1980). Hydrous melting would also result in higher degrees of partial melting such that high-Mg magmas can be produced (cf., Hirose and Kawamoto, 1995). However, Ca behaves differently from Mg and Fe during partial melting because of different partition coefficient in minerals. MgO and FeO increase with increasing degrees of partial melting, whereas CaO in the melts would reach the highest contents (~13%) when the degree of partial melting is 15–20% (Hirose and Kawamoto, 1995). Thus, the low-Ca SHMB-like parental magma of Huangshandong might have resulted from hydrous partial melting of depleted mantle under relatively low degrees of partial melting (~10%).

6.5. Tectonic settings of the Huangshandong intrusion

Extensive Permian magmatism has produced numerous mafic–ultramafic intrusions in the Tianshan Orogenic Belt. The petrogenesis

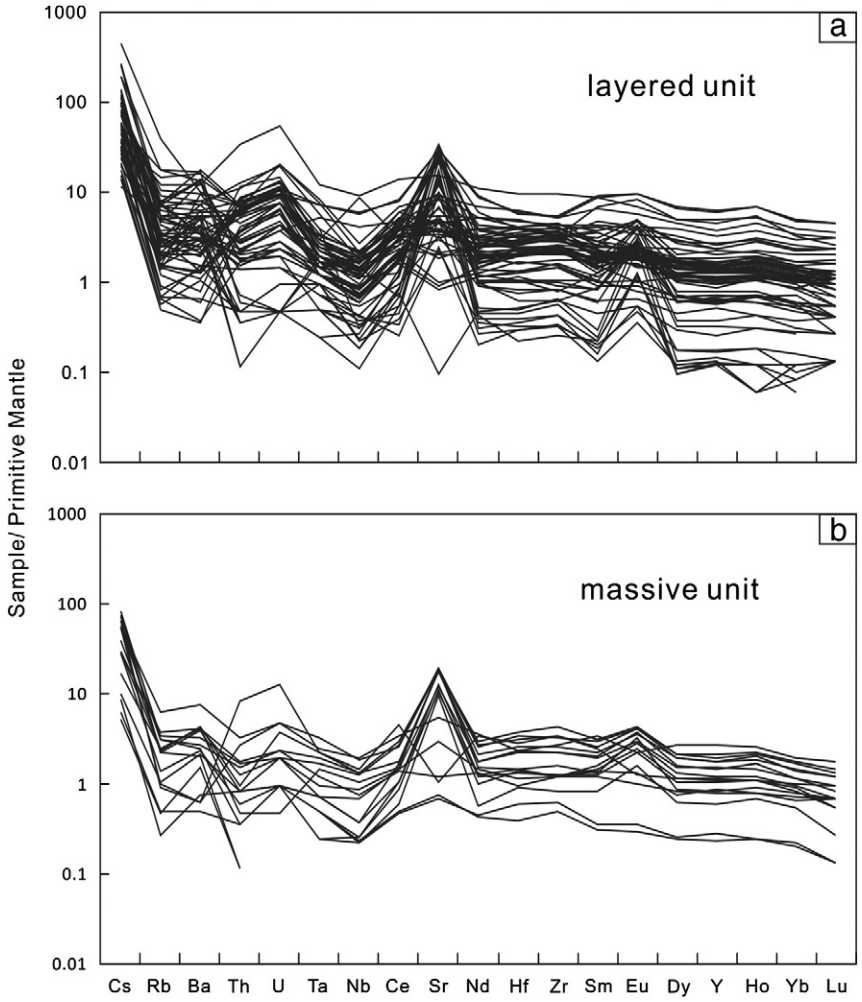

Fig. 8. Primitive-mantle normalized trace element patterns of (a) layered unit, and (b) massive unit. Normalization values are from Sun and McDonough (1989).

of these intrusions has been a matter of debate, with possible mechanisms including subduction, mantle-plume and post-collision extension for the origin of these intrusions.

Han et al. (2010) and Su et al. (2011b) considered that some mafic intrusions in this area are Alaskan-type intrusion and formed in a subduction zone environment. The widely spread coeval mafic and felsic intrusions in the Tianshan Orogenic Belt are also thought to be due to mantle-plume activity (Mao et al., 2008; Pirajno et al., 2008; Qin et al., 2011; Shan et al., 2009; Su et al., 2011a; Zhang et al., 2011). However, rocks of the Huangshandong intrusion are rich in orthopyroxene and so cannot be considered to be of Alaskan-type (c.f. Himmelberg and Loney, 1995). Alternatively, we propose that the parental magmas of the Huangshandong intrusion were produced by low-degrees of partial melting of a hydrous mantle source, and is

Table 3
Sr–Nd isotope of the Huangshandong rocks and ores.

Sample	Unit	Rb (ppm)	Sr (ppm)	$^{87}Rb/^{86}Sr$	$^{87}Sr/^{86}Sr$	2σ (10^{-6})	$^{87}Sr/^{86}Sr_i$	Sm (ppm)	Nd (ppm)	$^{147}Sm/^{144}Nd$	$^{143}Nd/^{144}Nd$	2σ (10^{-6})	$^{143}Nd/^{144}Nd_t$	$\varepsilon_{Nd(t)}$
HS813	MU	1.55	415	0.011	0.703059	9	0.7030	1.16	3.69	0.1981	0.513026	7	0.512677	7.5
HS927	MU	1.81	269	0.019	0.703109	11	0.7030	0.50	1.91	0.1650	0.512891	6	0.512600	6.0
HS932	MU	1.40	387	0.010	0.703081	11	0.7030	0.60	2.07	0.1824	0.512963	2	0.512642	6.8
HS820	LU	3.06	574	0.015	0.703847	6	0.7038	3.01	8.19	0.2316	0.512876	13	0.512292	3.4
HS920	LU	4.77	635	0.021	0.703835	10	0.7038	3.94	12.0	0.2074	0.512864	14	0.512499	4.0
HS924	LU	0.96	722	0.004	0.703147	12	0.7031	1.24	4.47	0.1753	0.512902	8	0.512593	5.9
HS901	LU	4.31	94	0.130	0.704357	2	0.7039	0.99	4.01	0.1558	0.512834	18	0.512560	5.2
HS906	LU	2.01	44	0.128	0.704819	6	0.7043	0.87	3.26	0.1691	0.512844	9	0.512546	5.0
HS917	LU	3.07	115	0.075	0.703945	5	0.7037	2.05	6.89	0.1874	0.512852	13	0.512522	4.5
HS952	LU	11.1	638	0.049	0.704087	11	0.7039	0.38	1.36	0.1783	0.512827	17	0.512513	4.3
HS832	LU	4.50	257	0.049	0.703615	7	0.7034	0.72	2.30	0.1963	0.512953	11	0.512607	6.2
HS828	LU	0.94	19.0	0.140	0.704302	7	0.7038	0.69	1.94	0.2238	0.512901	15	0.512507	4.2
HS934	LU	1.34	619	0.006	0.703647	10	0.7036	0.37	1.34	0.1723	0.512865	14	0.512562	5.3
HS940	LU	1.14	479	0.007	0.703790	12	0.7038	0.11	0.61	0.1163	0.512860	13	0.512655	7.1
HS830	LU	7.56	318	0.067	0.703858	8	0.7036	3.83	15.1	0.1599	0.512891	3	0.512609	6.2
HS843	LU	0.97	464	0.006	0.703662	12	0.7036	1.15	3.98	0.1821	0.512838	10	0.512517	4.4

Note: MU — massive unit; LU — layered unit.

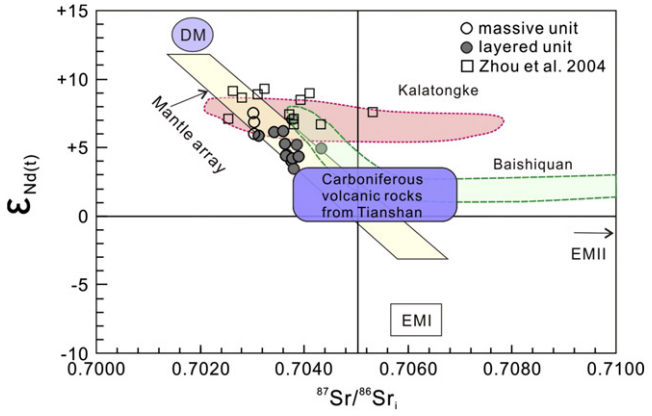

Fig. 9. Plot of $\varepsilon_{Nd\ (269\ Ma)}$ vs initial $^{87}Sr/^{86}Sr$ for the Huangshandong Intrusion (reference fields are after Zindler and Hart, 1986).

likely to have resulted from decompression melting rather than melting of a hot mantle plume. We thus suggest that the Huangshandong intrusion was formed in a post-collisional environment.

6.6. Implications for the genesis of SHMB-like magmas in orogenic belts

The Huangshandong intrusion is considered to have formed from two pulses of SHMB-like magmas. The earlier magma pulse was sulfide-saturated by crustal contamination and small proportion of sulfides ± olivine has been removed before it was emplaced into the magma chamber (Fig. 11). The later pulse of magma was more evolved, but did not undergo sulfide saturation and thus was Ni-undepleted SHMB-like magma (Fig. 11).

Assimilation and fractional crystallization of high-Mg basaltic or picritic magma can form SHMB magmas (Seitz and Keays, 1997; Srivastava, 2006; Srivastava and Gautam, 2009; Srivastava and Singh, 1999; Srivastava et al., 2010; Sun et al., 1991; Zhou et al., 2000). On the other hand, hydrous partial melting of depleted mantle can also produce SHMB-like magmas (Hatton and Sharpe, 1989; Redman and Keays, 1985). Previous models for the formation of SHMB include melting of depleted mantle in a fore arc setting to form boninites (Hamlyn and Keays, 1986; Hatton and Sharpe, 1989; Redman and Keays, 1985), crustally contaminated high-Mg basaltic magmas (Arndt and Jenner, 1986; Sun et al., 1989), and modification of magmas through crust–mantle interaction (Sensarma et al., 2002). Our identification of SHMB-like magmas in a Paleozoic orogenic belt suggests that SHMB-like magmas can be generated in a post-collisional environment.

Although it is still a matter of debate, the final amalgamation of the Tianshan Orogenic Belt is likely to have occurred in the late Carboniferous

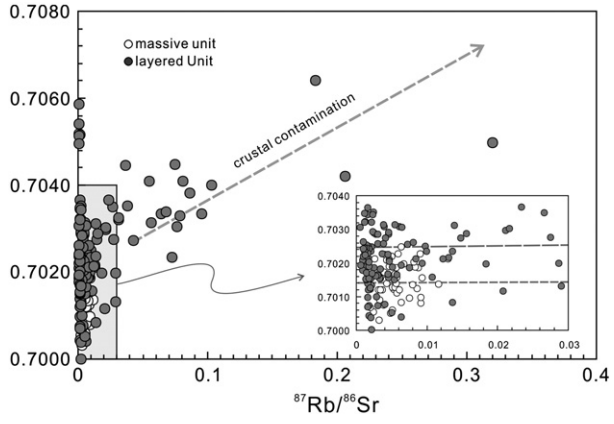

Fig. 10. In-situ $^{87}Sr/^{86}Sr$ ratios vs $^{87}Rb/^{86}Sr$ ratios for plagioclase from the Huangshandong intrusion.

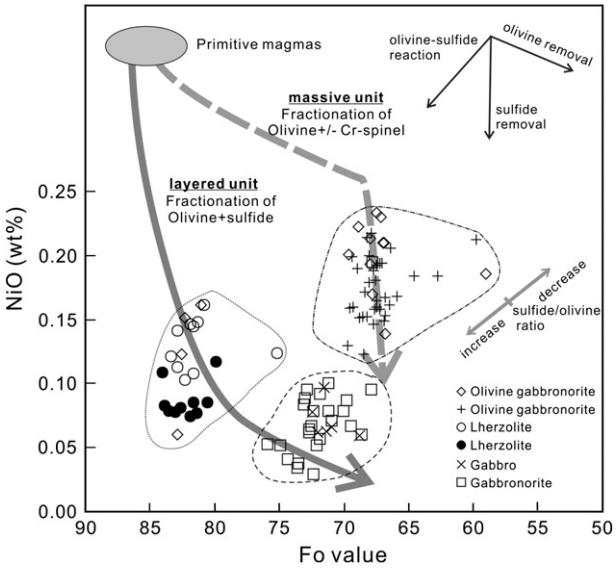

Fig. 11. Genetic model of the formation of two different parental magmas of the Huangshandong intrusion.

or early Permian and was followed by post-collisional extension (Zhou et al., 2004). Large scale post-collisional mafic and felsic magmatism in the southern margin of CAOB including the Tianshan Orogenic Belt produced widespread Permian granitic plutons and mafic–ultramafic intrusions (Jahn et al., 2000; Li et al., 2006a; Pirajno et al., 2008). The mantle underneath the orogenic belt was likely modified by the previous subduction. Mafic–ultramafic intrusions in North Xinjiang include the Kalatongke intrusion in the Chinese Altay orogenic belt (Gao et al., 2012; Shan et al., 2009; Song and Li, 2009) and the Huangshanxi (Yang, 1996; Zhang et al., 2011; Zhou et al., 2004), Xiangshan (Han et al., 2010; Li et al., 2006b; Sun et al., 2008; Wang et al., 2009), Baishiquan (Chai et al., 2008), and Tulargen (San et al., 2010; Sun et al., 2008) intrusions in the Tianshan Orogenic Belt, have SHMB-like affinities. These intrusions have similar lithology and geochemistry and may have formed from compositionally similar magmas derived from a hydrous and depleted mantle source in a post-collisional environment.

Although the origin of these intrusions is still a matter of debate, they have geochemical features different from intrusions formed in rift tectonic settings, such as those from Noril'sk (Russia) and Voisey's Bay (Canada). Intrusions from Noril'sk, and Voisey's Bay all have widely varying Nd isotopes with ε_{Nd} values from −13 to +8, indicating different mantle sources and different degrees of crustal contamination, whereas mafic–ultramafic intrusions in the southern margin of CAOB generally have high and positive ε_{Nd} and low radiogenic Sr isotopic compositions. On the other hand, orthopyroxene-rich mafic intrusions have been reported in the Appalachian Orogen (Thompson, 1984), and Dabie Orogenic Belt (Jahn et al., 1999; Nie and Li, 1998; Zhao et al., 2011). These differences can be readily explained by relatively depleted mantle sources underneath orogenic belts. We speculate that SHMB-like magmatism may be a feature common to many orogenic belts, different from those in rifting environments.

7. Conclusions

The Huangshandong intrusion was derived from low-Ca SHMB-like parental magmas and was formed by the injection of two magma pulses. The first magma pulse reached sulfide-saturation during emplacement and underwent early sulfide removal and was thus high-Mg and Ni-depleted. The second magma pulse was low-Mg and Ni-undepleted after fractionation of olivine without significant removal of sulfide. SHMB-like mafic–ultramafic magmatism may be a common feature of orogenic belts, produced in hydrous and depleted mantle sources.

Supplementary data to this article can be found online at http://dx.doi.org/10.1016/j.lithos.2013.01.002.

Acknowledgments

This study was supported by grants from the Chinese National Basic Research Program of China (973 Program) (2011CB808903) and the research grant council of Hong Kong (HKU7070/12P) and a 973 match grant from CRCG of HKU. We thank Professor Changyi Jiang of Chang'an University of China and Mr. Liren Sun of the Tianlong Mine for sharing their knowledge about the local geology. Mr. Gang Deng of the Sixth team of the Geological Survey of Xinjiang was a very capable field assistant. We are also very grateful to Prof. Ru-Cheng Wang, Prof. Ai-Cheng Zhang, Prof. Xiao-Ming Chen and Miss Wei Pu of Nanjing University for their assistance with the lab work. A.C. Kerr, R.K. Srivastava and an anonymous reviewer are much appreciated for their critical and constructive comments on this paper.

References

Arndt, N.T., Jenner, G.A., 1986. Crustally contaminated komatiites and basalts from Kambalda, Western Australia. Chemical Geology 56, 229–255.
Boudier, F., 1991. Olivine xenocrysts in picritic magmas: an experimental and microstructural study. Contributions to Mineralogy and Petrology 109, 114–123.
Campbell, F.E., Roeder, P.L., 1968. The stability of olivine and pyroxene in the Ni–Mg–Si–O system. American Mineralogist 53, 257–268.
Chai, F., Zhang, Z., Mao, J., Dong, L., Zhang, Z., Wu, H., 2008. Geology, petrology and geochemistry of the Baishiquan Ni–Cu-bearing mafic–ultramafic intrusions in Xinjiang, NW China: implications for tectonics and genesis of ores. Journal of Asian Earth Sciences 32, 218–235.
Coleman, R.G., 1989. Continental growth of Northwest China. Tectonics 8, 621–635.
Deniel, C., 2009. Heterogeneous initial Sr isotope compositions of highly evolved volcanic rocks from the Main Ethiopian Rift, Ethiopia. Bulletin of Volcanology 71, 495–508.
Gao, J., Li, M.S., Xiao, X.C., Tang, Y.Q., He, G.Q., 1998. Paleozoic tectonic evolution of the Tianshan Orogen, northwestern China. Tectonophysics 287, 213–231.
Gao, J.-F., Zhou, M.F., Lightfoot, P.C., Wang, C.Y., Qi, L., 2012. Origin of PGE-poor and Cu-rich magmatic sulfides from the Kalatongke deposit, Xinjiang, NW China. Economic Geology 107, 481–506.
Ghiorso, M.S., Sack, R.O., 1995. Chemical mass-transfer in magmatic processes IV: a revised and internally consistent thermodynamic model for the interpolation and extrapolation of liquid–solid equilibria in magmatic systems at elevated-temperatures and pressures. Contributions to Mineralogy and Petrology 119, 197–212.
Gu, L.X., Zhang, Z.Z., Wu, C.Z., Tang, J.H., San, J.Z., Wang, C.S., Zhang, G.H., 2007. Permian geological, metallurgical and geothermal events of the Huangshan-Jing' erquan area, eastern Tianshan: indications for mantle magma intraplating and its effect on the crust. Acta Petrologica Sinica 23, 2869–2880.
Hamlyn, P.R., Keays, R.R., 1986. Sulfur saturation and 2-stage melts: application to the Bushveld Platinum metal deposits. Economic Geology 81, 1431–1445.
Han, B.F., Ji, J.Q., Song, B., Chen, L.H., Li, Z., 2004. SHRIMP zircon U–Pb ages of Kalatongke No. 1 and Huangshandong Cu–Ni-bearing mafic–ultramafic complexes, North Xinjiang, and geological implications. Chinese Science Bulletin 49, 2424–2429.
Han, C.M., Xiao, W.J., Zhao, G.C., Ao, S.J., Zhang, J., Qu, W.J., Du, A.D., 2010. In-situ U–Pb, Hf and Re–Os isotopic analyses of the Xiangshan Ni–Cu–Co deposit in Eastern Tianshan (Xinjiang), Central Asia Orogenic Belt: constraints on the timing and genesis of the mineralization. Lithos 120, 547–562.
Hatton, C.J., Sharpe, M.R., 1989. Significance and origin of boninite like rocks associated with the Bushveld Complex. In: Crawford, A.J. (Ed.), Boninites. Unwin Hyman, London, pp. 174–207.
Himmelberg, G.R., Loney, A.L., 1995. Characteristics and Petrogenesis of Alaskan-Type Ultramafic–Mafic Intrusions, Southeastern Alaska. , pp. 1–47.
Hirano, N., Yamamoto, J., Kagi, H., Ishii, T., 2004. Young, olivine xenocryst-bearing alkali-basalt from the oceanward slope of the Japan Trench. Contributions to Mineralogy and Petrology 148, 47–54.
Hirose, K., Kawamoto, T., 1995. Hydrous partial melting of lherzolite at 1 GPa: the effect of H_2O on the genesis of basaltic magmas. Earth and Planetary Science Letters 133, 463–473.
Hoatson, D.M., Keays, R.R., 1989. Formation of platiniferous sulfide horizons by crystal fractionation and magma mixing in the Munni-Munni layered intrusion, West Pilbara Block, Western Australia. Economic Geology 84, 1775–1804.
Jahn, B.-m, Wu, F., Lo, C.-H., Tsai, C.-H., 1999. Crust–mantle interaction induced by deep subduction of the continental crust: geochemical and Sr–Nd isotopic evidence from post-collisional mafic–ultramafic intrusions of the northern Dabie complex, central China. Chemical Geology 157, 119–146.
Jahn, B.M., Wu, F.Y., Chen, B., 2000. Granitoids of the Central Asian Orogenic Belt and continental growth in the Phanerozoic. Transactions of the Royal Society of Edinburgh: Earth Sciences 91, 181–193.
Jaques, A.L., Green, D.H., 1980. Anhydrous melting of peridotite at 0–15 kb pressure and the genesis of tholeiitic basalts. Contributions to Mineralogy and Petrology 73, 287–310.
Kamenetsky, V.S., Elburg, M., Arculus, R., Thomas, R., 2006. Magmatic origin of low-Ca olivine in subduction-related magmas: co-existence of contrasting magmas. Chemical Geology 233, 346–357.
Keays, R.R., 1987. Principles of mobilization (dissolution) of metals in mafic and ultramafic rocks — the role of immiscible magmatic sulphides in the generation of hydrothermal gold and volcanogenic massive sulphide deposits. Ore Geology Reviews 2, 47–63.
Keays, R.R., 1995. The role of komatiitic and picritic magmatism and S-saturation in the formation of ore deposits. Lithos 34, 1–18.
Knesel, K.M., Davidson, J.P., Duffield, W.A., 1999. Evolution of silicic magma through assimilation and subsequent recharge: evidence from Sr isotopes in sanidine phenocrysts, Taylor Creek rhyolite, NM. Journal of Petrology 40, 773–786.
Li, C., Naldrett, A.J., 1999. Geology and petrology of the Voisey's Bay intrusion: reaction of olivine with sulfide and silicate liquids. Lithos 47, 1–31.
Li, C.D., Mou, J., Lan, G., Sun, Y., Yang, Z.X., Tang, J., Chen, J.F.M., Xiao, Y., 1996. Origin and Ore-Forming Principals of the Huangshan Cu–Ni Metallogenic Belt, Hami, Xinjiang. Press of Chengdu University of Sciences and Technology, Chengdu, p. 204.
Li, C.S., Ripley, E.M., Naldrett, A.J., 2003. Compositional variations of olivine and sulfur isotopes in the Noril'sk and Talnakh intrusions, Siberia: implications for ore-forming processes in dynamic magma conduits. Economic Geology and the Bulletin of the Society of Economic Geologists 98, 69–86.
Li, J.Y., Song, B., Wang, K.Z., Li, Y.P., Sun, G.H., Qi, D.Y., 2006a. Permian mafic–ultramafic complexes on the southern margin of the Tu-Ha Basin, East Tianshan Mountains: geological records of vertical crustal growth in Central Asia. Acta Geoscientia Sinica 27, 424–446.
Li, Y.C., Zhao, G.C., Qu, W.J., Pan, C.Z., Mao, Q.G., Du, A.D., 2006b. Re–Os isotopic dating of the Xiangshan deposit, East Tianshan, NW China. Acta Petrologica Sinica 22, 245–251.
Libourel, G., 1999. Systematics of calcium partitioning between olivine and silicate melt: implications for melt structure and calcium content of magmatic olivines. Contributions to Mineralogy and Petrology 136, 63–80.
Ma, R.S., Shu, L.S., Sun, J., 1997. Tectonic Evolution and Metallogenic of Eastern Tianshan Mountains. Geological Publishing House, Beijing.
Maier, W.D., Barnes, S.J., 2010. The Kabanga Ni sulfide deposits, Tanzania: II. Chalcophile and siderophile element geochemistry. Mineralium Deposita 45, 443–460.
Mao, J.W., Yang, J.M., Qu, W.J., Du, A.D., Wang, Z.L., Han, C.M., 2003. Re–Os age of Cu–Ni ores from the Huangshandong Cu–Ni sulfide deposit in the East Tianshan Mountains and its implication for geodynamic processes. Acta Geologica Sinica; English Edition 77, 220–226.
Mao, J.W., Pirajno, F., Zhang, Z.H., Chai, F.M., Wu, H., Chen, S.P., Cheng, L.S., Yang, J.M., Zhang, C.Q., 2008. A review of the Cu–Ni sulphide deposits in the Chinese Tianshan and Altay orogens (Xinjiang Autonomous Region, NW China): principal characteristics and ore-forming processes. Journal of Asian Earth Sciences 32, 184–203.
Nie, Y., Li, S., 1998. Sm–Nd age of syncollisional mafic–ultramafic intrusions in the Dabie Mountains. Chinese Science Bulletin 43, 160–163.
Pirajno, F., Mao, J., Zhang, Z., Zhang, Z., Chai, F., 2008. The association of mafic–ultramafic intrusions and A-type magmatism in the Tian Shan and Altay orogens, NW China: implications for geodynamic evolution and potential for the discovery of new ore deposits. Journal of Asian Earth Sciences 32, 165–183.
Pouchou, J.L., Pichoir, F., 1991. Quantitative-Analysis of Homogeneous or Stratified Microvolumes Applying the Model PAP.
Qi, L., Hu, J., Gregoire, D.C., 2000. Determination of trace elements in granites by inductively coupled plasma mass spectrometry. Talanta 51, 507–513.
Qin, K.Z., Su, B.X., Sakyi, P.A., Tang, D.M., Li, X.H., Sun, H., Xiao, Q.H., Liu, P.P., 2011. SIMS zircon U–Pb geochronology and Sr–Nd isotopes of Ni–Cu-bearing mafic–ultramafic intrusions in eastern Tianshan and Beishan in correlation with flood basalts in Tarim Basin (NW china): constraints on a ca. 280 Ma mantle plume. American Journal of Science 311, 237–260.
Ramos, F.C., Wolff, J.A., Tollstrup, D.L., 2004. Measuring Sr-87/Sr-86 variations in minerals and groundmass from basalts using LA-MC-ICPMS. Chemical Geology 211, 135–158.
Ramsay, W.R.H., Crawford, A.J., Foden, J.D., 1984. Field setting, mineralogy, chemistry, and genesis of arc picrites, New Georgia, Solomon Islands. Contributions to Mineralogy and Petrology 88, 386–402.
Redman, B.A., Keays, R.R., 1985. Archaean basic volcanism in the Eastern Goldfields Province, Yilgarn Block, Western Australia. Precambrian Research 30, 113–152.
Roeder, P.L., Emslie, R.F., 1970. Olivine-liquid equilibrium. Contributions to Mineralogy and Petrology 29, 275.
San, J., Qin, K., Tang, Z., Tang, D., Su, B., Sun, H., Xiao, Q., Liu, P., 2010. Precise zircon U–Pb age dating of two mafic–ultramafic complexes at Tulargen large Cu–Ni district and its geological implications. Acta Petrologica Sinica 26, 3027–3035.
Seitz, H.M., Keays, R.R., 1997. Platinum group element segregation and mineralization in a Noritic ring complex formed from Proterozoic siliceous high magnesium basalt magmas in the Vestfold Hills, Antarctica. Journal of Petrology 38, 703–725.
Sengör, A.M.C., Natalin, B.A., Burtman, V.S., 1993. Evolution of the Altaid tectonic collage and Paleozoic crustal growth in Eurasia. Nature 364, 299–307.
Sensarma, S., Palme, H., Mukhopadhyay, D., 2002. Crust–mantle interaction in the genesis of siliceous high magnesian basalts: evidence from the Early Proterozoic Dongargarh Supergroup, India. Chemical Geology 187, 21–37.
Shan, Q., Zhang, B., Luo, Y., Zhou, C.P., Yu, X.Y., Zeng, Q.S., Yang, W.B., Niu, H.C., 2009. Characteristics and trace element geochemistry of pyrite from the Songhu iron deposit, Nilek County, Xinjiang, China. Acta Petrologica Sinica 25, 1456–1464.
Song, X.-Y., Li, X.-R., 2009. Geochemistry of the Kalatongke Ni–Cu–(PGE) sulfide deposit, NW China: implications for the formation of magmatic sulfide mineralization in a postcollisional environment. Mineralium Deposita 44, 303–327.
Srivastava, R.K., 2006. Geochemistry and petrogenesis of Neoarchaean high-Mg low-Ti mafic igneous rocks in an intracratonic setting, Central India craton: evidence for boninite magmatism. Geochemical Journal 40, 15–31.

Srivastava, R.K., 2008. Global intracratonic boninite-norite magmatism during the Neoarchean-Paleoproterozoic: evidence from the central Indian Bastar craton. International Geology Review 50, 61–74.
Srivastava, R.K., Gautam, G.C., 2009. Precambrian mafic magmatism in the Bastar craton, central India. Journal of the Geological Society of India 73, 52–72.
Srivastava, R.K., Singh, R.K., 1999. Petrology and geochemistry of the Late Archaean siliceous high-magnesian basalts (SHMB) from Kaklur, southern Bastar craton, central India. Journal of the Geological Society of India 53, 693–704.
Srivastava, R.K., Mondal, S.K., Balaram, V., Gautam, G.C., 2010. PGE geochemistry of low-Ti high-Mg siliceous mafic rocks within the Archaean Central Indian Bastar Craton: implications for magma fractionation. Mineralogy and Petrology 98, 329–345.
Su, B.-X., Qin, K.-Z., Sakyi, P.A., Li, X.-H., Yang, Y.-H., Sun, H., Tang, D.-M., Liu, P.-P., Xiao, Q.-H., Malaviarachchi, S.P.K., 2011a. U–Pb ages and Hf–O isotopes of zircons from Late Paleozoic mafic–ultramafic units in the southern Central Asian Orogenic Belt: tectonic implications and evidence for an Early-Permian mantle plume. Gondwana Research 20, 516–531.
Su, B.-X., Qin, K.-Z., Sakyi, P.A., Malaviarachchi, S.P.K., Liu, P.-P., Tang, D.-M., Xiao, Q.-H., Sun, H., Ma, Y.-G., Mao, Q., 2011b. Occurrence of an Alaskan-type complex in the Middle Tianshan Massif, Central Asian Orogenic Belt: inferences from petrological and mineralogical studies. International Geology Review 54, 249–269.
Sun, S.S., McDonough, W.F., 1989. Chemical and isotopic systematics of oceanic basalts: implications for mantle composition and processes. In: Saunders, A.D., Norry, M.S. (Eds.), Magmatism in the Ocean Basins, vol. 42. Geological Society of London, Special Publication, pp. 313–345.
Sun, S.S., Nesbitt, R.W., McCulloch, M.T., 1989. Geochemistry and petrogenesis of Archaean and early Proterozoic siliceous high-magnesian basalts. In: Crawford, A.J. (Ed.), Boninites. Unwin Hyman, London, pp. 148–173.
Sun, S.S., Wallace, D.A., Hoatson, D.M., Glikson, A.Y., Keays, R.R., 1991. Use of geochemistry as a guide to platinum group element potential of mafic–ultramafic rocks: examples from the west Pilbara Block and Halls Creek Mobile Zone, Western Australia. Precambrian Research 50, 1–35.
Sun, H., Qin, K.Z., Li, J.X., Tang, D.M., Fan, X., Xiao, Q.H., 2008. Constraint of mantle partial melting on PGE mineralization of mafic–ultramafic intrusions in Eastern Tianshan: case study on Tulargen and Xiangshan Cu–Ni deposits. Acta Petrologica Sinica 24, 1079–1086.
Thompson, J.F.H., 1984. Acadian synorogenic mafic intrusions in the Maine Appalachians. American Journal of Science 284, 462–483.
Wang, C.Y., Zhou, M.F., 2006. Genesis of the Permian Baimazhai magmatic Ni–Cu–(PGE) sulfide deposit, Yunnan, SW China. Mineralium Deposita 41, 771–783.
Wang, C.Y., Zhou, M.F., Keays, R.R., 2006a. Geochemical constraints on the origin of the Permian Baimazhai mafic–ultramafic intrusion, SW China. Contributions to Mineralogy and Petrology 152, 309–321.
Wang, Y.W., Wang, J.B., Wang, L.J., 2006b. Comparison of host rocks between two vanadic titianomagnetite deposit types from the eastern Tianshan mountains. Acta Petrologica Sinica 22, 1425–1436.
Wang, Y.W., Wang, J.B., Wang, L.J., Long, L., 2009. Characteristics of two mafic–ultramafic rock series in the Xiangshan Cu–Ni–(V) Ti–Fe ore district, Xinjiang. Acta Petrologica Sinica 25, 888–900.
Windley, B.F., Allen, M.B., Zhang, C., Zhao, Z.Y., Wang, G.R., 1990. Paleozoic accretion and cenozoic redeformation of the Chinese Tien-shan-range, Central-Asia. Geology 18, 128–131.
Windley, B.F., Kroner, A., Guo, J.H., Qu, G.S., Li, Y.Y., Zhang, C., 2002. Neoproterozoic to Paleozoic geology of the Altai orogen, NW China: new zircon age data and tectonic evolution. Journal of Geology 110, 719–737.
Wolff, J.A., Ramos, F.C., Davidson, J.P., 1999. Sr isotope disequilibrium during differentiation of the Bandelier Tuff: constraints on the crystallization of a large rhyolitic magma chamber. Geology 27, 495–498.
Wu, F.Y., Wilde, S.A., Zhang, G.L., Sun, D.Y., 2004. Geochronology and petrogenesis of the post-orogenic Cu–Ni sulfide-bearing mafic–ultramafic complexes in Jilin Province, NE China. Journal of Asian Earth Sciences 23, 781–797.
Xia, M.Z., Jiang, C.Y., Qian, Z.Z., Xia, Z.D., Wang, B.Y., Sun, T., 2010. Geochemistry and petrogenesis of Huangshandong intrusion, East Tianshan, Xinjiang. Acta Petrologica Sinica 26, 2413–2430.
Yang, Z.X., 1996. Lithogenic and Metallogenic Dynamics of Mafic Magma in Huangshan Region. Chengdu University of Technology, Chengdu, China (133pp.).
Yang, Y., Wu, F., Xie, L., Yang, J., Zhang, Y., 2009. In-situ Sr isotopic measurement of natural geological samples by LA-MC-ICP-MS. Acta Petrologica Sinica 25, 3431–3441.
Zhang, Z.H., Mao, J.W., Du, A.D., Pirajno, F., Wang, Z.L., Chai, F.M., Zhang, Z.C., Yang, J.M., 2008. Re–Os dating of two Cu–Ni sulfide deposits in northern Xinjiang, NW China and its geological significance. Journal of Asian Earth Sciences 32, 204–217.
Zhang, M.J., Li, C.S., Fu, P.A.E., Hu, P.Q., Ripley, E.M., 2011. The Permian Huangshanxi Cu–Ni deposit in western China: intrusive–extrusive association, ore genesis, and exploration implications. Mineralium Deposita 46, 153–170.
Zhao, Z.-F., Zheng, Y.-F., Wei, C.-S., Wu, F.-Y., 2011. Origin of postcollisional magmatic rocks in the Dabie orogen: implications for crust–mantle interaction and crustal architecture. Lithos 126, 99–114.
Zhou, M.-F., Zhao, T.-P., Malpas, J., Sun, M., 2000. Crustal-contaminated komatiitic basalts in Southern China: products of a Proterozoic mantle plume beneath the Yangtze Block. Precambrian Research 103, 175–189.
Zhou, M.F., Lesher, C.M., Yang, Z.X., Li, J.W., Sun, M., 2004. Geochemistry and petrogenesis of 270 Ma Ni–Cu–(PGE) sulfide-bearing mafic intrusions in the Huangshan district, Eastern Xinjiang, Northwest China: implications for the tectonic evolution of the Central Asian orogenic belt. Chemical Geology 209, 233–257.
Zindler, A., Hart, S., 1986. Chemical geodynamics. Annual Review of Earth and Planetary Sciences 14, 493–571.